

Axial Creeping Flow in the Gap between a Rigid Cylinder and a Concentric Elastic Tube

S. B. Elbaz and A. D. Gat

Faculty of Mechanical Engineering, Technion - Israel Institute of Technology, Haifa 32000, Israel

(Received 2015)

We examine transient axial creeping flow in the annular gap between a rigid cylinder and a concentric elastic tube. The gap is initially filled with a thin fluid layer. The study focuses on viscous-elastic time-scales for which the rate of solid deformation is of the same order-of-magnitude as the velocity of the fluid. We employ an elastic shell model and the lubrication approximation to obtain a forced nonlinear diffusion equation governing the viscous-elastic interaction. In the case of an advancing liquid front into a configuration with a negligible film layer (compared with the radial deformation of the elastic tube), the governing equation degenerates into a forced porous medium equation, for which several closed-form solutions are presented. In the case where the initial film layer is non-negligible, self-similarity is used to devise propagation laws for a pressure driven liquid front. When advancing external forces are applied on the tube, the formation of dipole structures is shown to dominate the initial stages of the induced flow and deformation regimes. These are variants of the dipole solution of the porous medium equation. Finally, since the rate of pressure propagation decreases with the height of the liquid film, we show that isolated moving deformation patterns can be created and superimposed to generate a moving wave-like deformation field. The presented interaction between viscosity and elasticity may be applied to fields such as soft-robotics and micro-scale or larger swimmers by allowing for the time-dependent control of an axisymmetric compliant boundary.

1. Introduction

We examine the effect of elasticity on transient axial creeping flow in the annular gap between a rigid cylinder and a concentric elastic tube. Specifically, we aim to analyze nonlinear viscous-elastic dynamics where the elastic deformation significantly changes the boundaries of the flow. The gap between the cylinder and tube is assumed small compared to the radius and length of the cylinder. The flow-field is modeled by applying the lubrication approximation, while the external elastic tube is modeled by thin shell theory. We focus on viscous-elastic time-scales for which the rate of solid deformation is of the same order-of-magnitude as the velocity of the flow.

A similar configuration was examined by Paidoussis (1998) who focused on high Reynolds numbers. The interaction of elastic tubes and thin viscous flows, at the limit of low Reynolds numbers, has been studied by Halpern & Grotberg (1992) and White & Heil (2005) who, among others, analyzed the dynamics of a liquid film coating the inner surface of an elastic tube in the context of flows in small airways in the lungs. Other studies involving a thin creeping flow between a rigid surface and an elastic surface focused on

planar configurations. These include Chauhan & Radke (2002), who modeled the dynamics of a contact lens during blinking as a thin viscous film contained between an elastic shell and a flat rigid surface. Pihler-Puzović *et al.* (2012) and Al-Housseiny *et al.* (2013) studied the effect of elasticity on the onset of Taylor-Saffman fingering instability in Hele-Shaw cells. Pihler-Puzović *et al.* (2014) related the patterns of viscous fingering to patterns of wrinkling in an elastic Hele-Shaw cell. Trinh *et al.* (2014*a*) and Trinh *et al.* (2014*b*) studied rigid and elastic plates, either pinned or free floating, moving over a viscous film laying on a flat rigid surface. Carlson *et al.* (2015) studied the deformation and flow-field created by a propagating adhesion front attaching an elastic sheet to a rigid surface, where the gap between the elastic sheet and rigid surface is filled with a viscous fluid.

For the case in which there is initially a vanishingly small gap between the rigid cylinder and the elastic tube, the examined problem can be viewed as a cylindrical version of the peeling problem (McEwan & Taylor 1966; Hosoi & Mahadevan 2004; Lister *et al.* 2013). In this regard the peeling formation of the current study bears mathematical proximity to a viscous gravity current (e.g., Buckmaster 1977; Huppert 1982; Momoniat 2006). Gravity currents have also been studied in geophysical contexts when coupled with elastic surfaces (Howell *et al.* 2013; Hewitt *et al.* 2015; Balmforth *et al.* 2015).

To the best of our knowledge, the problem examined in this work has not previously been studied. The suggested configuration may have bearing on models of compliant boundaries (Gad-el Hak 2002), axisymmetric swimmers and soft robotic applications. The structure of this work is as follows: In §2 the geometry, relevant parameters and physical assumptions are defined. In §3 elastic shell theory and the lubrication approximation are employed to obtain a forced nonlinear diffusion equation governing the viscous-elastic interaction. §4 examines an advancing liquid front in the limit of an initial vanishingly small gap (viscous peeling) where the governing equation simplifies to a porous medium equation. In §5 the self-similar scheme of the porous medium equation is modified to account for a pre-wetted gap between the cylinder and tube. In §6 the dipole solution of the porous medium equation is related to the pressure and deformation field created in the initial stages of the response to an advancing external pressure acting on the elastic tube. §7 examines isolated moving deformations for the case of relative axial speed between the rigid cylinder and the elastic tube. §8 presents concluding remarks.

2. Problem formulation

We study Newtonian, incompressible axial creeping flow in the annular gap between a rigid cylinder and a concentric linearly elastic tube. The gap between the cylinder and tube is assumed small compared to the radius of the cylinder. The flow is driven by time-varying pressures at the inlet or outlet, relative axial speed between the centre-body (cylinder) and elastic tube, as well as an external pressure field acting on the elastic tube. We examine transient dynamics in the viscous-elastic time-scale, where the rate of elastic deformation is of the same order-of-magnitude as the fluid velocity. We assume sufficient height of the liquid filled gap between the tube and centre-body, so that Van-der-Waals forces between the solids can be neglected. While §4-7 deal with configurations with constant radii of the centre-body and tube when at rest, in §2-3 we allow for small axial variations of the configuration (see Fig. 1).

Hereafter, normalized variables are denoted by uppercase letters and characteristic parameters are denoted by lowercase letters with asterisks (e.g., if a is a dimensional variable, a^* is the characteristic value of a and $A = a/a^*$ is the corresponding normalized variable).

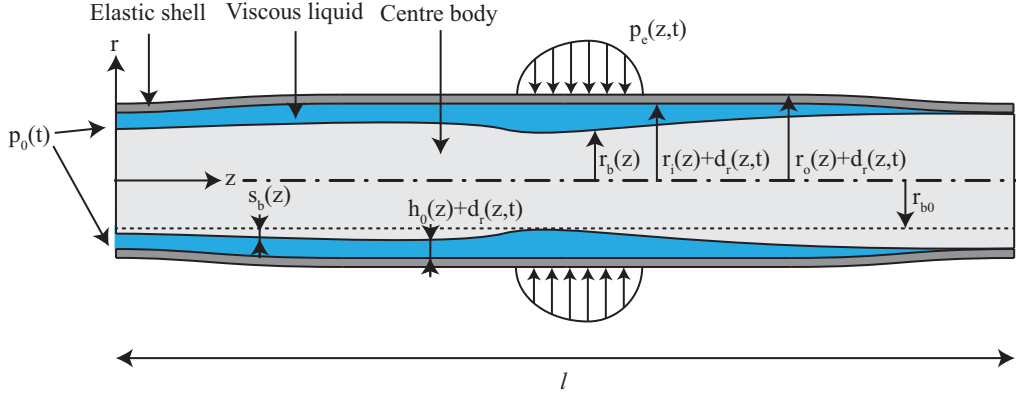


Figure 1: Schematic illustration of the elastic tube and annular fluid layer enclosing a weakly varying cross-section rigid centre-body. We define the cylindrical coordinates (r, z) . p_e is the external pressure field, and d_r, d_z are radial and axial solid deformations, respectively. $r_b(z)$ is the radius of the centre-body, r_{b0} is the minimal value of $r_b(z)$ and $s_b(z) = r_b(z) - r_{b0}$. $r_i(z) + d_r(z, t)$ and $r_o(z) + d_r(z, t)$ are the inner and outer surfaces of the elastic tube, respectively. $h_0(z) + d_r(z, t)$ is the annular gap between the inner centre-body and the elastic tube. $p_0(t)$ is an arbitrary time varying inlet pressure.

The relevant variables and parameters are time t , axial coordinate z , radial coordinate r , axial liquid speed u_z , radial liquid speed u_r , liquid pressure p , liquid viscosity μ , liquid density ρ , solid axial deformation d_z , solid radial deformation d_r , solid strain e_{ij} and stress σ_{ij} (acting on the plane normal to coordinate i and in the direction of coordinate j), solid Young's modulus E , solid Poisson's ratio ν , external shell (tube) inner contour $r_i(z)$ and outer contour $r_o(z)$ (see Fig. 1), external shell midsection, $r_m(z) = (r_i(z) + r_o(z))/2$, centre-body contour radius $r_b(z)$ and the length of the configuration in the z direction, l .

The gap (at rest) between the inner body and tube is defined as $h_0(z) = r_i(z) - r_b(z)$. We define the auxiliary radial coordinate, $s = r - r_b(z)$. The base radius of the inner-body is defined by $r_{b0} = \min(r_b(z))$ and the corresponding function describing the centre-body radius is $s_b(z) = r_b(z) - r_{b0}$. We define the slenderness ratio of the configuration as $\epsilon = r_{b0}/l$. The ratio of characteristic fluid layer thickness at rest to characteristic radial deformation is defined by $\lambda_h = h_0^*/d_r^*$ and the ratio of mean centre-body depth in excess of the base radius to characteristic radial deformation is defined by $\lambda_b = s_b^*/d_r^*$.

We define normalized coordinates, $(R, Z) = (r/r_{b0}, z/l)$, normalized radial and axial deflections, $(D_r, D_z) = (d_r/d_r^*, d_z/d_z^*)$, normalized liquid pressure, $P = p/p^*$ and external domain pressure, $P_e = p_e/p^*$, where p^* is the characteristic pressure, and normalized liquid velocity $(U_r, U_z) = (u_r/u_r^*, u_z/u_z^*)$, with corresponding characteristic values u_r^* and u_z^* .

Small parameters in the analysis include the ratio between the change in centre-body cross-section and the length of the geometry in the z direction,

$$\frac{dr_b}{dz} \sim \frac{s_b^*}{l} \ll 1, \quad (2.1)$$

and the ratio between the characteristic radial deformation d_r^* and the length of the geometry in the z direction, i.e., the fluidic aspect ratio,

$$\frac{d_r^*}{l} = \epsilon_1 \ll 1. \quad (2.2)$$

We utilize a thin elastic shell approximation and thus require the ratio of wall thickness $r_o - r_i$ to inner tube radius r_i to be small,

$$\frac{r_o - r_i}{r_i} = \varepsilon_2 \ll 1, \quad (2.3)$$

as well as small elastic deformations, expressed by the ratios,

$$\frac{d_r^*}{r_i} \sim \frac{d_z^*}{l} = \varepsilon_3 \ll 1. \quad (2.4)$$

Our analysis also assumes negligible inertia, represented by the condition,

$$Re_r = \frac{d_r^* \rho u_z^* d_r^*}{l \mu} \ll 1. \quad (2.5)$$

A more detailed discussion of the condition of negligible inertia is presented in §3.4.

3. Obtaining the leading order governing equation of the viscous-elastic dynamics

In order to obtain the governing viscous-elastic interaction equation, we apply the lubrication approximation for the flow field and the Kirchhoff-Love thin shell approximation for the solid deformation field, under the requirement of similar time-scales of both elastic and fluidic dynamics.

While the elastic shell configuration is similar to our previous work (Elbaz & Gat 2014), the characteristic shear stress σ_{zr}^* applied by the liquid on the solid is $O(\varepsilon_3)$ smaller compared with the characteristic shear obtained in Elbaz & Gat (2014), (this is readily seen from order-of-magnitude analysis of an integral force balance $p^* d_r^* 2\pi r_i \sim \sigma_{zr}^* l 2\pi r_i$). We thus redevelop the thin shell approximation herein.

3.1. The elastic problem

The deformation field of axisymmetric linearly elastic material with negligible inertia is governed by the momentum equations,

$$\frac{\partial}{\partial r}(r\sigma_{rr}) + \frac{\partial}{\partial z}(r\sigma_{zr}) - \sigma_{\theta\theta} = 0, \quad \frac{\partial}{\partial r}(r\sigma_{zr}) + \frac{\partial}{\partial z}(r\sigma_{zz}) = 0, \quad (3.1)$$

the strain-displacement relations,

$$e_{rr} = \frac{\partial d_r}{\partial r}, \quad e_{\theta\theta} = \frac{d_r}{r}, \quad e_{zz} = \frac{\partial d_z}{\partial z}, \quad e_{zr} = \frac{1}{2} \left(\frac{\partial d_r}{\partial z} + \frac{\partial d_z}{\partial r} \right), \quad (3.2)$$

and Hooke's law,

$$Ee_{zr} = (1 + \nu)\sigma_{zr}, \quad Ee_{rr} = \sigma_{rr} - \nu(\sigma_{zz} + \sigma_{\theta\theta}), \quad Ee_{\theta\theta} = \sigma_{\theta\theta} - \nu(\sigma_{rr} + \sigma_{zz}), \quad (3.3a)$$

$$Ee_{zz} = \sigma_{zz} - \nu(\sigma_{rr} + \sigma_{\theta\theta}). \quad (3.3b)$$

The boundary conditions for the stress applied by the liquid at $r = r_i + d_r$ are

$$\sigma_{rr}(r = r_i + d_r) = -p + 2\mu \frac{\partial u_r}{\partial r}, \quad \sigma_{zr}(r = r_i + d_r) = -\mu \left(\frac{\partial u_z}{\partial r} + \frac{\partial u_r}{\partial z} \right), \quad (3.4a)$$

and at $r = r_o + d_r$ the externally applied stress is

$$\sigma_{rr}(r = r_o + d_r) = -p_e, \quad \sigma_{zr}(r = r_o + d_r) = 0. \quad (3.4b)$$

Following elastic shell theory (Mollmann 1981), we define stress resultants for the forces n_{ij} and moments m_{ij} as

$$n_{ij} = \int_{r_i}^{r_o} \sigma_{ij} dr, \quad m_{ij} = \int_{r_i}^{r_o} \sigma_{ij} r dr. \quad (3.5)$$

The curvature of the external shell dr_m/dz will introduce only negligible terms, of order $O(\varepsilon_1)$, in the stress resultants (3.5). However, centre-body curvature dr_b/dz will have leading order effects in the fluidic analysis (§3.2). We multiply the axial momentum equation by $r - r_m$ and integrate over r to obtain a resultant form. We then differentiate with respect to z in order to relate to the radial momentum equation (3.1). This yields

$$\frac{\partial n_{zr}}{\partial z} - \frac{\partial^2 m_{zz}}{\partial z^2} + r_i \frac{\partial \sigma_{zr}(r_i)}{\partial z} = O(\varepsilon_2). \quad (3.6)$$

Substituting into the resultant form of the radial momentum equation,

$$r_i p - r_o p_e + r_i \left(\frac{\partial^2 m_{zz}}{\partial z^2} - r_i \frac{\partial \sigma_{zr}(r_i)}{\partial z} \right) - n_{\theta\theta} = O(\varepsilon_2). \quad (3.7)$$

Order-of-magnitude analysis of the axial momentum equation in (3.1) yields a relation between characteristic values,

$$n_{zz}^* = d_r^* p^*, \quad \sigma_{zz}^* = \frac{p^*}{\varepsilon_2} \varepsilon_3, \quad (3.8)$$

and order-of-magnitude analysis of (3.7) yields

$$n_{\theta\theta}^* = r_{b0} p^*, \quad \sigma_{\theta\theta}^* = \frac{p^*}{\varepsilon_2}. \quad (3.9)$$

The shear and normal stress characteristic values, $\sigma_{rr}^* = p^*$ and $\sigma_{zr}^* = \varepsilon_1 p^*$ are obtained from the fluidic problem (see §3.2).

Taking note that $m_{zz}^* = r_{b0} n_{zz}^*$, normalizing (3.7) yields in leading order,

$$N_{\theta\theta} = P - P_e + O(\varepsilon_1 \varepsilon, \varepsilon_2), \quad (3.10)$$

and normalizing Hooke's law (3.3) according to the above characteristic values yields a reduced form of Love's first approximation (Love 1888),

$$\Sigma_{\theta\theta} \sim -\frac{E\varepsilon_2}{p^* \nu} e_{zz} \sim \frac{E\varepsilon_2}{p^*} e_{\theta\theta}, \quad (3.11)$$

for which orders of $O(\varepsilon_2, \varepsilon_3)$ are neglected and $\Sigma_{\theta\theta} = \sigma_{\theta\theta}/(p^*/\varepsilon_2)$. We apply (Dugdale & Ruiz 1971) the Kirchhoff hypothesis and describe the displacement field in terms of the radial \bar{d}_r and axial \bar{d}_z displacements of the midsection, denoted by overbars,

$$\bar{d}_z = d_z + (r - r_m) \frac{\partial d_r}{\partial z}, \quad \bar{d}_r = d_r, \quad (3.12)$$

and thus we can represent the strain as a function of the deformation by

$$e_{zz} = \frac{\partial \bar{d}_z}{\partial z} - (r - r_m) \frac{\partial^2 \bar{d}_r}{\partial z^2}, \quad e_{\theta\theta} = \frac{\bar{d}_r}{r}. \quad (3.13)$$

Integrating (3.11) over r into resultant form and substituting $N_{\theta\theta}$ from (3.10) provides the leading order fluidic pressure to elastic deformations relation,

$$\bar{D}_r = P - P_e, \quad \bar{D}_z - \bar{D}_z(Z=0) = -\nu \int_0^Z (P - P_e) dZ, \quad (3.14)$$

as well as a relation between the characteristic radial deformation and characteristic pressure,

$$\frac{p^*}{E\varepsilon_2} = \frac{d_r^*}{r_{b0}} = \varepsilon_3 \ll 1. \quad (3.15)$$

Equation (3.15) provides limitation on the maximal allowed pressure for which the assumption of small deformations is valid.

3.2. The fluidic problem

We assume an axisymmetric incompressible Newtonian fluid, governed by the momentum equations,

$$\rho \left(\frac{\partial u_r}{\partial t} + u_r \frac{\partial u_r}{\partial r} + u_z \frac{\partial u_r}{\partial z} \right) = -\frac{\partial p}{\partial r} + \mu \left[\frac{1}{r} \frac{\partial}{\partial r} \left(r \frac{\partial u_r}{\partial r} \right) + \frac{\partial^2 u_r}{\partial z^2} - \frac{u_r}{r^2} \right], \quad (3.16)$$

$$\rho \left(\frac{\partial u_z}{\partial t} + u_r \frac{\partial u_z}{\partial r} + u_z \frac{\partial u_z}{\partial z} \right) = -\frac{\partial p}{\partial z} + \mu \left[\frac{1}{r} \frac{\partial}{\partial r} \left(r \frac{\partial u_z}{\partial r} \right) + \frac{\partial^2 u_z}{\partial z^2} \right] + \rho g, \quad (3.17)$$

and conservation of mass,

$$\frac{1}{r} \frac{\partial}{\partial r} (r u_r) + \frac{\partial u_z}{\partial z} = 0. \quad (3.18)$$

The relevant boundary conditions are no-slip and no-penetration at $r = r_i + d_r$,

$$u_r(r = r_b + h_0 + d_r) = \frac{\partial d_r}{\partial t}, \quad u_z(r = r_b + h_0 + d_r) = \frac{\partial d_z}{\partial t}, \quad (3.19)$$

and at the centre-body boundary, $r = r_b$,

$$u_r(r = r_b) = 0, \quad u_z(r = r_b) = u_0. \quad (3.20)$$

Pressure at the inlet and outlet may be governed by

$$p(z = 0) = p_0(t), \quad p(z = l) = p_l(t), \quad (3.21)$$

where $p_0(t)$ and $p_l(t)$ are arbitrary functions of time. We normalize the coordinate $s = r - r_b(z)$, defined in the gap $0 \leq s \leq h_0(z) + d_r(z, t)$, by d_r^* ,

$$S = \frac{s}{d_r^*}, \quad 0 \leq S \leq \lambda_h H_0(Z) + D_r(Z, T), \quad (3.22)$$

where $H_0 = h_0/h_0^*$. Based on (3.22) we can relate the normalized radial coordinate R to S ,

$$R = 1 + \varepsilon_3 (S + \lambda_b S_b(Z)), \quad (3.23)$$

where $S_b(Z) = s_b(z)/s_b^*$. Order-of-magnitude analysis of (3.18) yields

$$\frac{u_r^*}{u_z^*} \sim \frac{d_r^*}{l} = \varepsilon_1, \quad u_z^* = \frac{\varepsilon_1 d_r^* p^*}{\mu}. \quad (3.24)$$

We require $u_0 \sim u_z^*$ so that the viscous stresses resulting from centre-body motion scale as $\mu u_0/d_r^*$. We focus on negligible gravity, $G = \rho g l/p^* \ll 1$, and define a reduced Reynolds number, $Re = \rho u_z^* d_r^*/\mu$, and Womersley number, $\alpha^2 = \rho d_r^{*2}/\mu t^*$. Applying transformation (3.23) to (3.16)-(3.18) and employing (3.24) yields the following reduced system for the fluidic domain,

$$\frac{\partial P}{\partial Z} = \frac{\partial^2 U_z}{\partial S^2} + O\left(\alpha^2, \varepsilon_3, \varepsilon_1 Re, \varepsilon_1^2, \lambda_b \frac{\partial P}{\partial S}, G\right), \quad (3.25a)$$

$$\frac{\partial P}{\partial S} = O(\alpha^2, \varepsilon_1^3 Re, \varepsilon_1^2), \quad (3.25b)$$

$$\frac{\partial U_r}{\partial S} - \lambda_b \frac{dS_b}{dZ} \frac{\partial U_z}{\partial S} + \frac{\partial U_z}{\partial Z} = O(\varepsilon_3). \quad (3.25c)$$

Equations (3.25) are valid for $\lambda_h, \lambda_b \sim 1$ and $\lambda_h, \lambda_b \ll 1$. t^* represents the time-scale of the viscous-elastic interaction and is to be obtained by relation to the elastic problem.

3.2.1. Nonlinear problem formulation

The boundary conditions (3.19), (3.20) take the normalized form,

$$U_r(S = \lambda_h H_0 + D_r) = \frac{d_r^*}{t^* u_r^*} \frac{\partial D_r}{\partial T}, \quad U_z(S = \lambda_h H_0 + D_r) = \frac{d_z^*}{t^* u_z^*} \frac{\partial D_z}{\partial T}, \quad (3.26a)$$

and

$$U_r(S = 0) = 0, \quad U_z(S = 0) = U_0, \quad (3.26b)$$

with $U_0 = u_0/u_z^*$ and $T = t/t^*$. We solve (3.25a), (3.25b) imposing conditions (3.26a), (3.26b). The resulting leading order axial speed U_z reads

$$U_z \sim \frac{1}{2} \frac{\partial P}{\partial Z} [S^2 - (\lambda_h H_0 + D_r)S] + \frac{S}{(\lambda_h H_0 + D_r)} \frac{d_z^*}{t^* u_z^*} \frac{\partial D_z}{\partial T} + U_0 \left[1 - \frac{S}{(\lambda_h H_0 + D_r)} \right], \quad (3.27)$$

and is defined for $\lambda_h H_0 + D_r > 0$. Addressing mass conservation (3.25c), we install (3.27) and integrate with respect to S across the film layer to produce a reduced Reynolds equation relating fluidic pressure to elastic deformations and curvature,

$$\begin{aligned} & \frac{d_r^*}{t^* u_r^*} \frac{\partial D_r}{\partial T} - \frac{1}{12} \frac{\partial}{\partial Z} \left\{ \frac{\partial P}{\partial Z} (\lambda_h H_0 + D_r)^3 \right\} + U_0 \left[\frac{1}{2} \frac{\partial}{\partial Z} (\lambda_h H_0 + D_r) + \lambda_b \frac{dS_b}{dZ} \right] \\ & + \frac{1}{2} \frac{d_z^*}{t^* u_z^*} \left[(\lambda_h H_0 + D_r) \frac{\partial^2 D_z}{\partial Z \partial T} - \left[\frac{\partial}{\partial Z} (\lambda_h H_0 + D_r) + 2\lambda_b \frac{dS_b}{dZ} \right] \frac{\partial D_z}{\partial T} \right] \sim 0. \end{aligned} \quad (3.28)$$

Equation (3.28) is valid for $\lambda_h H_0 + D_r > 0$ and must be zeroed for values of (Z, T) that render $\lambda_h H_0 + D_r \leq 0$, since fluid pressure cannot contract the tube beneath the centre-body surface. We are now in a position to evaluate the characteristic coefficients and hence the time-scale t^* . By dominant balance a consistent result is achieved by setting $t^* = d_r^*/u_r^*$. The residual axial speed terms, coefficients of $\partial D_z/\partial T$, are of order $O(\varepsilon_3)$. Thus (3.28) reduces to

$$\frac{\partial D_r}{\partial T} - \frac{1}{12} \frac{\partial}{\partial Z} \left\{ \frac{\partial P}{\partial Z} (\lambda_h H_0 + D_r)^3 \right\} + U_0 \left[\frac{1}{2} \frac{\partial}{\partial Z} (\lambda_h H_0 + D_r) + \lambda_b \frac{dS_b}{dZ} \right] \sim 0. \quad (3.29)$$

3.2.2. Linear problem formulation

In the case of large $\lambda_h = h_0^*/d_r^* \gg 1$ the characteristic gap should be defined by h_0^* and not d_r^* . This requires renormalization of the lubrication approximation attained in (3.25a)-(3.25c). The renormalized parameters associated with the linear problem, denoted by the tilde symbol, are given by In the case of large $\lambda_h = h_0^*/d_r^* \gg 1$ the characteristic gap should be defined by h_0^* and not d_r^* . This requires renormalization of the lubrication approximation attained in (3.25a)-(3.25c). The renormalized parameters associated with the linear problem, denoted by the tilde symbol, are given by

$$\tilde{\varepsilon}_1 = \lambda_h \varepsilon_1, \quad \tilde{\varepsilon}_3 = \lambda_h \varepsilon_3, \quad \tilde{\lambda}_b = \lambda_h^{-1} \lambda_b, \quad \tilde{Re} = \lambda_h Re, \quad \tilde{\alpha} = \lambda_h \alpha. \quad (3.30)$$

We renormalize the local film coordinate and domain,

$$\tilde{S} = \lambda_h^{-1} S, \quad 0 \leq \tilde{S} \leq H_0(Z) + \lambda_h^{-1} D_r(Z, T), \quad (3.31)$$

and reapply boundary conditions (3.26a)-(3.26b) in \tilde{S} . The characteristic radial and axial velocities now scale as $u_r^*/u_z^* \sim \tilde{\varepsilon}_1$ and $u_z^* = \tilde{\varepsilon}_1 h_0^* p^*/\mu$. The reduced equations of motion for the linear case may be rewritten in tilde form,

$$\frac{\partial P}{\partial \tilde{Z}} = \frac{\partial^2 U_z}{\partial \tilde{S}^2} + O\left(\tilde{\alpha}^2, \tilde{\varepsilon}_3, \tilde{\varepsilon}_1 \tilde{R}e, \tilde{\varepsilon}_1^2, \tilde{\lambda}_b \frac{\partial P}{\partial \tilde{S}}, G\right), \quad (3.32a)$$

$$\frac{\partial P}{\partial \tilde{S}} = O\left(\tilde{\alpha}^2, \tilde{\varepsilon}_1^3 \tilde{R}e, \tilde{\varepsilon}_1^2\right), \quad (3.32b)$$

$$\frac{\partial U_r}{\partial \tilde{S}} - \tilde{\lambda}_b \frac{dS_b}{dZ} \frac{\partial U_z}{\partial \tilde{S}} + \frac{\partial U_z}{\partial \tilde{Z}} = O(\tilde{\varepsilon}_3). \quad (3.32c)$$

Following a similar procedure to that of §3.2.1 we derive a linearized reduced Reynolds equation analogous to (3.29),

$$\frac{\partial D_r}{\partial T} - \frac{1}{12} \frac{\partial}{\partial \tilde{Z}} \left\{ \frac{\partial P}{\partial \tilde{Z}} (H_0 + \lambda_h^{-1} D_r)^3 \right\} + U_0 \left[\frac{1}{2} \frac{\partial}{\partial \tilde{Z}} (H_0 + \lambda_h^{-1} D_r) + \tilde{\lambda}_b \frac{dS_b}{dZ} \right] \sim 0. \quad (3.33)$$

3.3. The fluidic-elastic problem

We substitute (3.14) into (3.29) dropping the midsection overbars and derive an initial boundary value problem for the nonlinear viscous-elastic interaction (for the corresponding dimensional equation see equation A 1 of Appendix A),

$$\frac{\partial(P - P_e)}{\partial T} - \frac{1}{12} \frac{\partial}{\partial Z} \left\{ \frac{\partial P}{\partial Z} (\lambda_h H_0 + P - P_e)^3 \right\} + U_0 \left[\frac{1}{2} \frac{\partial}{\partial Z} (\lambda_h H_0 + P - P_e) + \lambda_b \frac{dS_b}{dZ} \right] \sim 0, \quad (3.34)$$

with corresponding centre-body surface condition rewritten in pressure form,

$$P > P_e - \lambda_h H_0. \quad (3.35)$$

Equations (3.34)-(3.35) may be solved with an initial condition $P(Z, 0) = P_i(Z)$ and boundary conditions of type (3.21) in normalized form $P(0, T) = P_0(T)$, $P(1, T) = P_1(T)$. The characteristic time-scale t^* of the nonlinear viscous-elastic interaction is evaluated via relations (3.15) and (3.24),

$$t^* = \frac{(E\varepsilon_2)^2 \mu}{p^{*3} \varepsilon^2}. \quad (3.36)$$

The dependence in characteristic pressure stems from the pressure dependent diffusion coefficient of (3.34).

As per the linear case, all elastic analysis results of §3.1 hold with substituted tilde parameters of (3.30) where applicable. Therefore an analogous substitution of (3.14) into (3.33) will yield the corresponding linear initial boundary value problem for inlet pressure driven viscous-elastic perturbations of the external shell,

$$\begin{aligned} & \frac{\partial(P - P_e)}{\partial T} - \frac{1}{12} \frac{\partial}{\partial Z} \left\{ \frac{\partial P}{\partial Z} (H_0 + \lambda_h^{-1} (P - P_e))^3 \right\} \\ & + U_0 \left[\frac{1}{2} \frac{\partial}{\partial Z} (H_0 + \lambda_h^{-1} (P - P_e)) + \tilde{\lambda}_b \frac{dS_b}{dZ} \right] \sim 0. \end{aligned} \quad (3.37)$$

With corresponding initial and boundary conditions. The characteristic time-scale t^* is

reevaluated for the linear case,

$$t^* = \frac{\mu}{E\tilde{\varepsilon}_1^2\tilde{\varepsilon}_3\varepsilon_2}, \quad (3.38)$$

and shows exclusive dependence in solid-liquid material properties and the geometry of the configuration. A result which is consistent with the linear interaction time-scale of the full cross-section cylindrical shell (Elbaz & Gat 2014).

3.4. Non-linearity and neglected inertia terms

Equating the non-linear time-scale, (3.36) and linear time-scale, (3.38) we derive a condition on the characteristic pressure for which the system will exhibit nonlinear behavior,

$$p^* \geq E\lambda_h\varepsilon_2\varepsilon_3 = E\frac{r_o - r_i}{r_i}\frac{h_0^*}{r_i}. \quad (3.39)$$

As the pre-wetting layer vanishes, $h_0^* \rightarrow 0$, any small perturbation in pressure will propagate nonlinearly, representing a state for which the problem is not linearizable. There is an upper limit on the characteristic pressure beyond which the assumption of negligible inertia (3.25a)-(3.25b) will no longer be valid, representing the range of validity of the analysis. Substituting (3.36) into (3.25a), we demand that both α^2 and $\varepsilon_1 Re$ terms be negligible and derive the condition that

$$p^* \ll \left(\frac{\mu}{\varepsilon r_{b0}}\right)^{\frac{2}{5}} \frac{(E\varepsilon_2)^{\frac{4}{5}}}{\rho^{\frac{1}{5}}}. \quad (3.40)$$

It will be shown in §5 that the transition from a nonlinear to a linear regime occurs quite rapidly in the intermediate λ_h range.

4. Closed-form solution of the peeling problem and derivation of propagation laws

At the limit $\lambda_h \rightarrow 0$ while setting $P_e = U_0 = 0$, (3.34) describes cylindrical pressure-driven viscous peeling of the external shell from the centre-body and reduces to the porous medium equation (PME) in fourth power,

$$\frac{\partial P}{\partial T} - \frac{\partial^2 P^4}{\partial Z^2} \sim 0, \quad (4.1)$$

with adjusted time-scale, $T = t/\kappa t^*$, $\kappa = 48$. We transform to self-similar variables,

$$P = T^{-\alpha} f(\eta), \quad \eta = ZT^{\frac{3\alpha-1}{2}}, \quad (4.2)$$

and adopt Huppert's renormalization (Huppert 1982) in light of the close mathematical analogy to a viscous gravity current propagating under a density gradient,

$$F(\xi) = \eta_F^{-\frac{2}{3}} f(\eta), \quad \eta = \eta_F \xi. \quad (4.3)$$

η_F describes the propagating peeling front for which the solution is supported in the region $Z < Z_F(T)$, prior to boundary interaction $Z_F(T) < 1$. We install (4.2), (4.3) into (4.1) which then reduces to the following ODE in F ,

$$(F^4)'' + \left(\frac{1-3\alpha}{2}\right)\xi F' + \alpha F \sim 0. \quad (4.4)$$

The eigenvalue α describes the inlet pressure boundary condition,

$$P(0, T) = T^{-\alpha}, \quad (4.5)$$

and thus,

$$F(0) = \eta_F^{-\frac{2}{3}}, \quad F(\xi \geq 1) = 0. \quad (4.6)$$

We complete the formulation with integral mass conservation represented in non-dimensional form by

$$\int_0^{Z_F(T)} P(Z, T) dZ = QT^{\frac{1-5\alpha}{2}}, \quad Q = \eta_F^{\frac{5}{3}} \int_0^1 F(\xi) d\xi. \quad (4.7)$$

Both η_F and Q are functions of the eigenvalue α . Contrary to a viscous gravity current where the interface is induced by a given flux input, in which case the flux rate Q may be set constant for all α , in the current study the flux rate derives from the inlet pressure.

Eq. (4.4) is solved analytically for $\alpha = 1/5$ and is a particular case of the source solution of the PME, known as the ZKB solution, as first obtained by Zeldovich & Kompaneets (1950) and Barenblatt (1952). The underlying boundary and initial conditions are

$$P(Z, 0) = Q\delta(Z), \quad \frac{\partial P(0, T)}{\partial Z} = 0, \quad (4.8)$$

representing a sudden input of mass, Q , into the interface at $T = 0$, after which the inlet is sealed. The amplitude decay at the inlet, as the front spreads through the interface, is then given by (4.5). The solution reads

$$P(Z, T) = T^{-\frac{1}{5}} \left[1 - \frac{3}{40} Z^2 T^{-\frac{2}{5}} \right]_+^{\frac{1}{3}}, \quad Q = \frac{\sqrt{\frac{10\pi}{3}} \Gamma(\frac{4}{3})}{\Gamma(\frac{11}{6})}, \quad \eta_F = \sqrt{\frac{40}{3}}, \quad (4.9)$$

where $(s)_+ = \max(s, 0)$ and Γ is Euler's Gamma function. The velocity field corresponding to (4.9) can be attained via (3.27) and (3.25c). The dimensional solution corresponding to (4.9) is given by (A 2). For all other physical values of α ($\alpha < 1/5$) (4.4), along with conditions (4.6) and (4.7), is solved numerically. In the range $\alpha \leq 0$ the underlying initial condition is $P(Z, 0) = 0$. Fig. 2(a) presents the self-similar pressure profile $F(\xi)$ for $\alpha = 1/5$ (4.9) and for $\alpha = 0, -1, -2, -3$ corresponding to inlet signals of type (4.5). Fig. 2(b) depicts the flux rate Q , the front locus η_F , and the time it takes the front to reach the opposite boundary, denoted T_b , as a function of α . Fig. 2(b) is plotted in the range $\alpha \leq 0$ (the range $0 < \alpha \leq 1/5$ is irrelevant for comparison due to the change in boundary and initial conditions). T_b represents the limit of validity of the self-similar analysis when adapted to a finite domain, it reaches a maxima around $\alpha = -1$ below which it decreases moderately. Figs. 2(c) and (d) depict the resulting deformation regime, D_z and D_r , respectively, for the case of constant boundary pressure ($\alpha = 0$). The peeling front enters from the left ($Z = 0$) while the tube is set stationary at the right end $D_r(1, T) = D_z(1, T) = 0$. The deformations are attained via (3.14), a strain ratio of $\varepsilon_3 = 0.25$ and a Poisson's ratio of $\nu = 0.5$ were used. As the front propagates the interface the tube shrinks from the free left end. The upper half of the radial deformation profile slightly steepens due to the D_z deformation field.

The propagation laws for an inlet signal of type (4.5), according to self-similarity, are written in terms of the front location Z_F , accumulated mass in the interface M , and time to boundary T_b ,

$$Z_F = \eta_F(\alpha) T^{\frac{1-3\alpha}{2}}, \quad M = Q(\alpha) T^{\frac{1-5\alpha}{2}}, \quad T_b = \eta_F(\alpha)^{-\frac{2}{1-3\alpha}}, \quad (4.10)$$

where $T = t/\kappa t^*$ and $\kappa = 48$. The corresponding dimensional propagation laws are given in (A 3). The spread rate of a disturbance in an unperturbed medium in the case of a full cross-section cylindrical shell containing a viscous liquid is of order $O(t^{1/2})$ (Elbaz & Gat 2014), and is independent of the inlet signal or the nature of the external

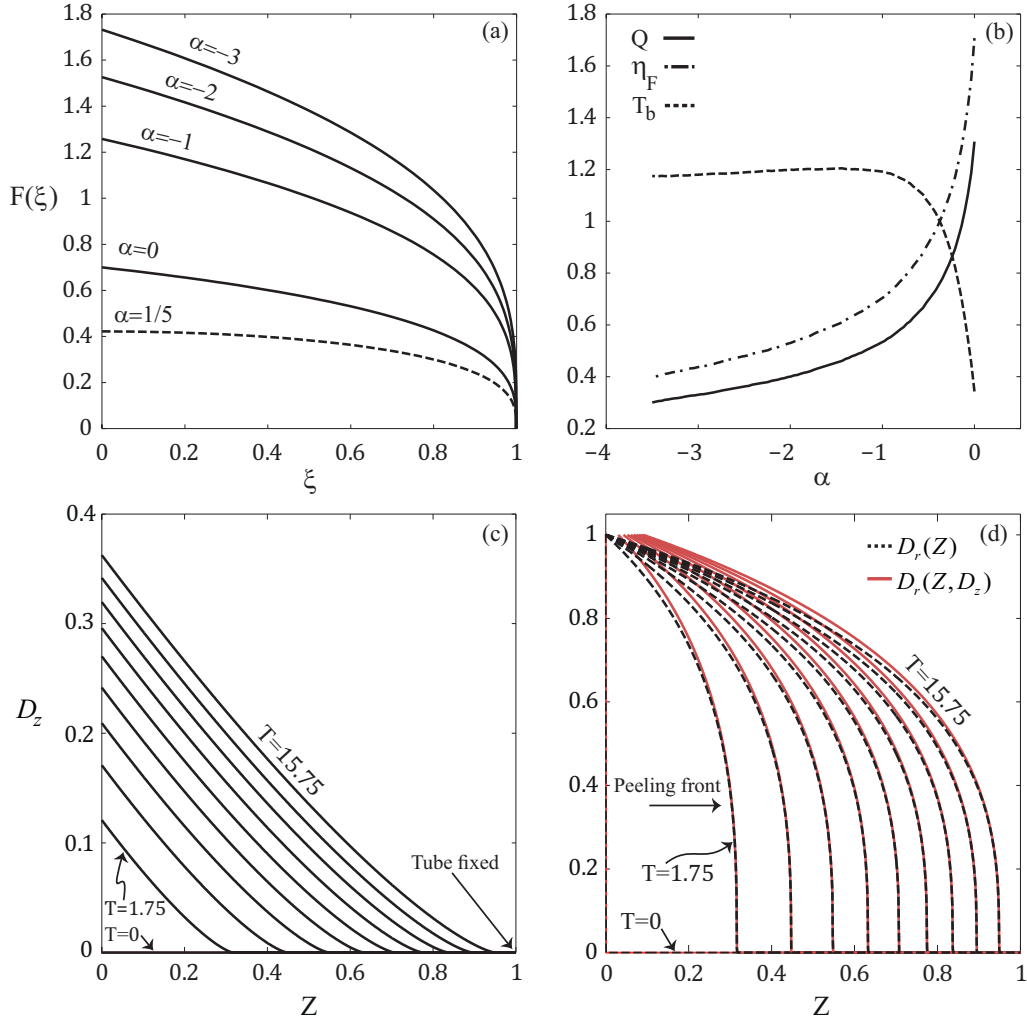


Figure 2: Self-similar solutions of cylindrical pressure driven viscous peeling, corresponding to $\lambda_h \rightarrow 0$, $P_e = U_0 = 0$ and inlet pressure $P(0, T) = T^{-\alpha}$. Part (a): Pressure profile $F(\xi)$ corresponding to eigenvalues: $\alpha = -1/5$ (analytic) - dashed line, $\alpha = 0, -1, -2, -3$ - solid lines (obtained numerically). Part (b): Flux rate $Q(\alpha)$ - solid line, front locus $\eta_F(\alpha)$ - dashed-dotted line, time to boundary $T_b(\alpha) = t_b/\kappa t^*$ - dashed line (Q, η_F and T_b obtained numerically). Parts (c,d): Constant boundary pressure viscous peeling ($\alpha = 0$), tube fixed at $Z = 1$, $D_r(1, T) = D_z(1, T) = 0$. Part (c): Axial deformation $D_z(Z, T)$, progressive snapshots of $\Delta T = 1.75$, between $0 \leq T \leq 15.75$, shown in the natural time-scale $T = t/t^*$. Part (d): Radial deformation $D_r(Z, T)$ vs. undeformed axial coordinate - dashed black, vs. deformed axial coordinate - solid red, progressive snapshots of $\Delta T = 1.75$, between $0 \leq T \leq 15.75$, shown in the natural time-scale $T = t/t^*$, $\varepsilon_3 = 0.25$, $\nu = 0.5$.

forcing, this is a linear property which stems from the heat kernel and applies to the linear interaction model of the current study (3.37). Thus, when comparing the spread rate of pressure driven viscous peeling with the propagation of a disturbance over a non-negligible fluid layer, we note that an impulse of type (4.8) is slower, $O(t^{1/5})$, than its linear counterpart for large enough time, and that otherwise faster rates can be achieved due to the dependence in inlet pressure.

5. Effect of pre-wetting layer, self-similar analysis and numerical solution

We consider a constant nonzero pre-wetting layer $\lambda_h > 0$, $H_0 = 1$, about a stationary cylindrical centre-body, with no external forcing $P_e = 0$. Eq. (3.34) reduces to

$$\frac{\partial P}{\partial T} - 4 \frac{\partial}{\partial Z} \left\{ \frac{\partial P}{\partial Z} (\lambda_h + P)^3 \right\} \sim 0, \quad (5.1)$$

with $T = t/\kappa t^*$ and $\kappa = 48$. We transform back to PME form, $\Phi = \lambda_h + P$,

$$\frac{\partial \Phi}{\partial T} - \frac{\partial^2 \Phi^4}{\partial Z^2} \sim 0. \quad (5.2)$$

Focusing on the case of constant boundary pressure driven peeling,

$$P(0, T) = 1, \quad P(Z, 0) = 0, \quad \alpha = 0, \quad (5.3)$$

the self-similar analysis of §4 may be extended to include the effect of the pre-wetting layer. We adopt the tilde symbol for all self-similar variables corresponding to a pre-wetting layer. Following §4, we substitute $\Phi = \tilde{\eta}_F^{-\frac{2}{3}} \tilde{F}(\tilde{\xi})$, and rewrite the boundary and initial condition in shifted pressure Φ in terms of the pre-wetted self-similar pressure profile \tilde{F} ,

$$\tilde{F}(0) = \tilde{\eta}_F^{-\frac{2}{3}} (1 + \lambda_h), \quad \tilde{F}(\tilde{\xi} \geq 1) = \tilde{\eta}_F^{-\frac{2}{3}} \lambda_h, \quad (5.4)$$

in similar fashion to (4.6). Since we are interested in values of λ_h for which $P(Z, T)$ maintains its compact support we must add the condition that,

$$\frac{d\tilde{F}(1)}{d\tilde{\xi}} = 0. \quad (5.5)$$

Integral mass conservation (4.7) becomes,

$$\int_0^{\tilde{Z}_F(T)} P(Z, T) dZ = \tilde{Q} T^{\frac{1}{2}}, \quad \tilde{Q} = \tilde{\eta}_F^{\frac{5}{3}} \int_0^1 \tilde{F}(\tilde{\xi}) d\tilde{\xi} - \lambda_h \tilde{\eta}_F, \quad (5.6)$$

where \tilde{Q} and $\tilde{\eta}_F$ are functions of the base layer thickness λ_h . The self-similar ODE ((4.4), at $\alpha = 0$) written in $\tilde{F}(\tilde{\xi})$ along with boundary conditions (5.4), (5.5) and (5.6) formulate an eigenvalue problem in λ_h . It is solved numerically with initial guess from §4 ($\alpha = 0$). The solution is presented in Fig. 3(a) and starts from the outer pressure profile of the unpenetrated interface ($\lambda_h = 0$) previously attained in §4. Subsequent profiles correspond to $\lambda_h = 0.2, 0.4, 0.6, 0.8$ and 1. Fig. 3(b) depicts the resulting flux rate \tilde{Q} , front locus $\tilde{\eta}_F$, and boundary time \tilde{T}_b , in the nonlinear scale range $0 \leq \lambda_h \leq 1$. We thus derive propagation laws for a constant boundary pressure viscous-elastic peeling front when spreading over a base layer. The front location \tilde{Z}_F , accumulated mass in the interface excluding the base layer \tilde{M} , and time to boundary \tilde{T}_b are given by,

$$\tilde{Z}_F = \tilde{\eta}_F(\lambda_h) T^{\frac{1}{2}}, \quad \tilde{M} = \tilde{Q}(\lambda_h) T^{\frac{1}{2}}, \quad \tilde{T}_b = \tilde{\eta}_F^{-2}(\lambda_h), \quad (5.7)$$

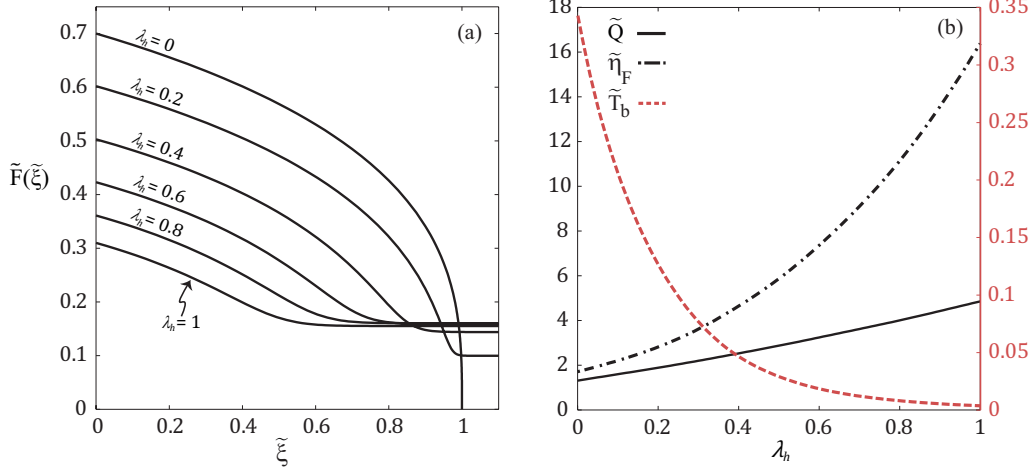


Figure 3: Self-similar solutions of cylindrical pressure driven viscous peeling over a pre-wetting layer for constant boundary pressure, corresponding to $0 \leq \lambda_h \leq 1$, $P_e = 0$ and inlet pressure $P(0, T) = 1$. Part (a): Shifted pressure profile $\tilde{F}(\tilde{\xi})$ corresponding to eigenvalues: $\lambda_h = 0, 0.2, 0.4, 0.6, 0.8, 1$ (obtained numerically). Part (b): Flux rate $\tilde{Q}(\lambda_h)$ - solid black line, front locus $\tilde{\eta}_F(\lambda_h)$ - dashed-dotted black line, time to boundary $\tilde{T}_b(\lambda_h) = \tilde{t}_b/\kappa t^*$ - dashed red line in right aligned scale (obtained numerically).

where $T = t/\kappa t^*$. In the presence of a base layer, the unpenetrated interface front of §4 ($\alpha = 0$) is accelerated by $\tilde{\eta}_F(\lambda_h)/\tilde{\eta}_F(0)$, resulting in faster boundary time \tilde{T}_b and an added mass of $\tilde{Q}(\lambda_h)/\tilde{Q}(0)$.

For nonzero λ_h (5.1) is no longer parabolic degenerate for $P = 0$ and therefore does not exhibit the orthogonal fronts of the PME (4.1). As λ_h grows, a larger $\tilde{\eta}_F$ is required to converge to a constant value at the right boundary ($\tilde{\xi} = 1$) causing the profiles to spread inward (see Fig. 3(a)). For $\lambda_h > 1$, \tilde{F} scales as,

$$\tilde{F}(\tilde{\xi}; \lambda_h) = O\left(\frac{\lambda_h}{\tilde{\eta}_F^{\frac{2}{3}}(\lambda_h)}\right), \quad \lambda_h > 1 \quad (5.8)$$

and ultimately vanishes as $\lambda_h \rightarrow \infty$. Thus, for $\lambda_h > 1$ the self-similar profiles of $\tilde{F}(\tilde{\xi})$ still provide an exact solution for $P(Z, T)$ albeit in a diminishing time frame $T < \tilde{T}_b$, representing the limit of the nonlinear interaction model when extended into the linear λ_h range. We'd like to emphasize that while constant boundary pressure driven peeling propagates as $O(t^{1/2})$ irrespective of the base layer thickness, this is not the case for other types of inlet signals. For example, source type boundary conditions (to be examined below (5.9)) transition from $O(t^{1/5})$ propagation for $\lambda_h \rightarrow 0$ to $O(t^{1/2})$ for $\lambda_h \rightarrow \infty$.

We illustrate the effect of a pre-wetting layer on the propagation of a source type viscous-elastic front via numerical solution of (5.1) (readjusted to the natural time-scale $T = t/t^*$) along with appropriate boundary conditions,

$$P(Z, 0) = \delta(Z), \quad \frac{\partial P(0, T)}{\partial Z} = \frac{\partial P(1, T)}{\partial Z} = 0. \quad (5.9)$$

A no flux condition at the right boundary has been added to demonstrate the interaction

of the front with the opposing wall, deemed to start around $T = \kappa T_b (\alpha = 1/5)$, for small enough values of λ_h . Propagation in time is shown in 3 progressive snapshots in Fig. 4(a),(b),(c) corresponding to $T = 0.012, 0.12, 0.6$, respectively, and for varying base layer thickness $0 \leq \lambda_h \leq 3/2$. The solution was obtained via a finite difference scheme and was validated on the basis of section §4. For $\lambda_h > 1$ the solution is presented in the nonlinear time scale normalization (3.36) for comparison. Acceleration of the front as well as its spreading is observed as the base layer thickens. At the physical limit of large λ_h the solution for source type boundary conditions (5.9), representing pressure driven viscous-elastic perturbations of the external shell, tends to the behavior of the heat equation, $\lambda_h \rightarrow \infty$ in (3.37), which converges exponentially and for which the transfer of information is no longer confined to a compact support of the solution, which generally travels immediately to the whole interface as of $T = 0$. Thus the solution of a propagating front or disturbance over a pre-wetting layer can be viewed as the synthesis of two fundamental solutions, the ZKB profiles of (4.9) and the Gaussian profiles akin to (3.37). As the base pressure falls below the crossover value of condition (3.39) the solution will increasingly exhibit linear behavior and vice versa.

6. Dipole structures and their role in the transient response to moving external forces

One of the fundamental solutions of the PME (4.1), as first attained by Zeldovich & Barenblatt (1957), is the dipole solution. It is constructed by taking the distributional spatial derivative of the delta function as initial condition, $P(Z, 0) = \partial\delta(Z)/\partial Z$, on the infinite line. The dipole solution has also been studied in the context of viscous gravity currents (King & Woods 2003), analogous to the configuration presented in §4. However, the peeling formation of §4 cannot sustain negative pressure values due to violation of the surface condition (3.35) and therefore cannot accommodate the classical dipole solution.

Let us examine governing equation (3.34) when forced by external pressure P_e . A non-negligible fluid layer resides in the annular gap $\lambda_h = 1, H_0 = 1$ and the centre-body is stationary $U_0 = 0$ and of zero curvature $dS_b/dZ = 0$. Hence (3.34) reads,

$$\frac{\partial P}{\partial T} - \frac{1}{12} \frac{\partial}{\partial Z} \left\{ \frac{\partial P}{\partial Z} (\lambda_h + P - P_e)^3 \right\} \sim \frac{\partial P_e}{\partial T}. \quad (6.1)$$

A structure similar to a dipole may occur when a high pressure region and a low pressure region form adjacent to one another while the diffusion coefficient (here $(\lambda_h + P - P_e)^3$) zeroes at the pivot (see Fig. 5(a)). Such conditions can be met at the transient phase of the response to an advancing spatially localized external force,

$$P_e(Z, T) = \delta(Z - 1/2 - \omega T). \quad (6.2)$$

Fig. 5(a) depicts the initial transient phase of the solution of equation (6.1) under these conditions, plotted between $0 \leq T \leq 0.012$ in $\Delta T = 0.002$ increments. The forcing (6.2) is implemented as a unit Gaussian so as to scale locally as the film layer λ_h , its width 0.1 and velocity $\omega = \pi$, as depicted in Fig. 5(b). Outside the dipole centre the base layer smooths out the pressure. As the external shock moves down the tube $T > 0.012$ the dipole structure will collapse and the system will transition into a new pressure and deformation regime.

While (6.2) is a specific case designed to create a dipole-like structure, dipoles are inherent to the initial stages of the response to externally moving forces, occurring in areas where the diffusion coefficient vanishes. We define a general external moving wave

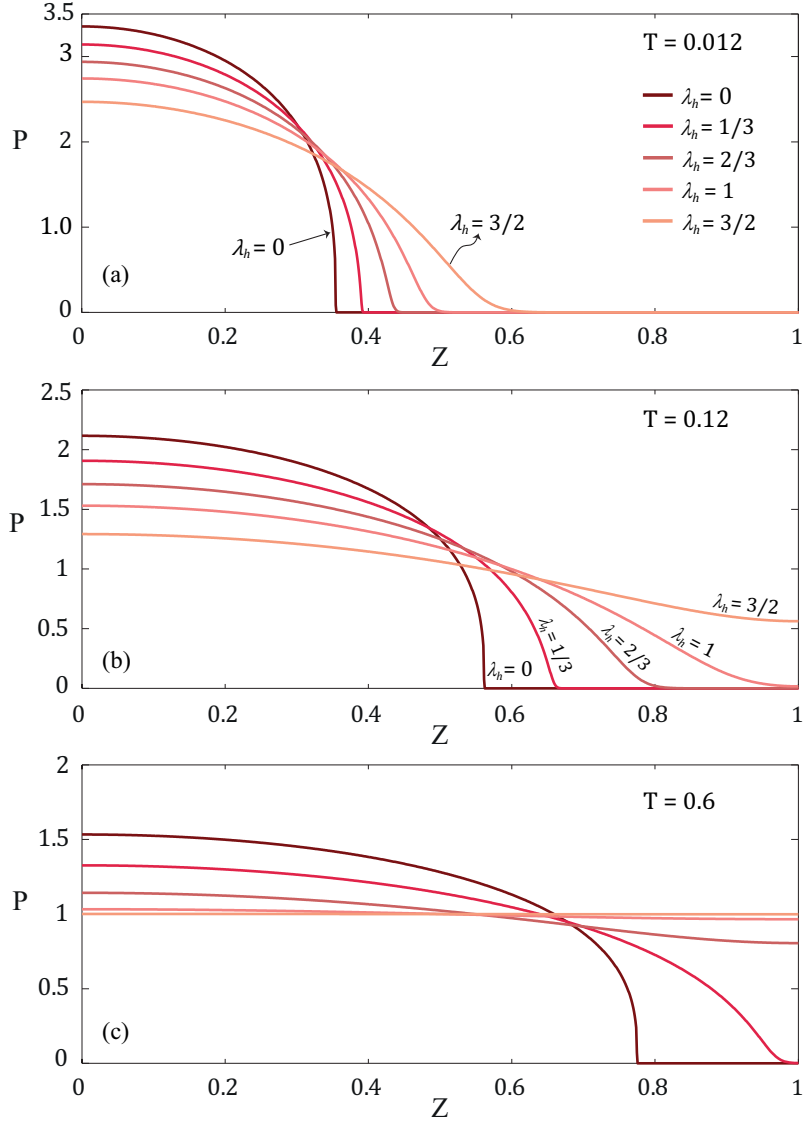


Figure 4: Nonlinear viscous-elastic interaction over a pre-wetting layer - source solution. Numerical solution corresponding to $0 \leq \lambda_h \leq 3/2, H_0 = 1, P_e = U_0 = 0, 0 \leq T \leq 0.6$. Pressure plotted vs. axial coordinate. Boundary conditions of type (5.9). $\lambda_h = 0, 1/3, 2/3, 1, 3/2$ from dark to light reds respectively. Part (a): solution at time $T=0.012$, Fig. Part (b): solution at time $T=0.12$, Part (c): solution at time $T=0.6$.

force of the form,

$$P_e(Z, T) = a \sin(kZ - \omega T). \quad (6.3)$$

Fig. 6 demonstrates this transient dipole formation for the case of $a = 1, k = 7\pi, \omega = 10\pi$, P_e plotted in Fig. 6(a) between $0 \leq T \leq 0.1$. A no-flux boundary condition was employed

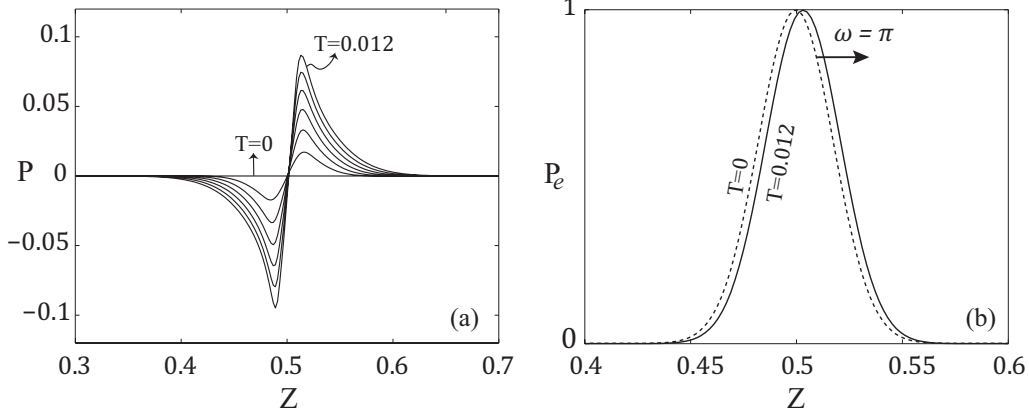


Figure 5: Initial transient phase dipole formation in response to an advancing spatially localized external force. Part (a): Fluid pressure dipole structure close-up, solution in $\Delta T = 0.002$ increments between $0 \leq T \leq 0.012$. Part (b): External pressure $P_e = \delta(Z - 1/2 - \omega T)$, implemented as a unit Gaussian, width 0.1, velocity $\omega = \pi$, $0 \leq T \leq 0.012$.

at either end of the tube,

$$\frac{\partial P(0, T)}{\partial Z} = \frac{\partial P(1, T)}{\partial Z} = 0, \quad (6.4)$$

representative of a closed system. The solution (see Fig. 6(b)) is plotted between $0 \leq T \leq 0.1$ in $\Delta T = 0.014$ increments. The outermost dipoles are strongly influenced by the boundary walls. The asymmetry of the central dipoles results from the simultaneity of the transient buildup and diffusion processes. Thus, the dipole structure is a fundamental mechanism of the transient response to external forcing and is essential when considering a pulsating external environment.

7. Transported ZKB profile, a building block for creating complex deformation patterns

In this section we illustrate the use of the transport term of (3.34) $\partial P / \partial Z \cdot U_0 / 2$, and the relation between the speed of pressure propagation and the gap (λ_h), in order to obtain isolated moving deformations. The linear transport term of equation (3.34) may represent a relative motion of the centre-body, or alternatively, $U_0(T)$ can be thought of as a slip velocity condition induced by an electric zeta potential or a similar mechanism. We set $P_e = 0$ and examine uniform geometry $H_0 = 1$, $dS_b/dZ = 0$, with a small pre-wetting layer $\lambda_h \ll 1$. Eq. (3.34) reduces to

$$\frac{\partial P}{\partial T} + \frac{U_0}{2} \frac{\partial P}{\partial Z} - \frac{1}{12} \frac{\partial}{\partial Z} \left\{ \frac{\partial P}{\partial Z} (\lambda_h + P)^3 \right\} \sim 0. \quad (7.1)$$

At the left boundary we employ an impulse sequence of the form,

$$P(0, T) = \sum_{n=0}^N A_n \left[\Theta \left(T + \frac{\Delta T_n}{2} - \tau_n \right) - \Theta \left(T - \frac{\Delta T_n}{2} - \tau_n \right) \right], \quad (7.2)$$

where Θ is the Heaviside function. The signal is modulated in amplitude, A_n , and in width ΔT_n and can be sequenced non-uniformly by τ_n . We set a zero initial condition

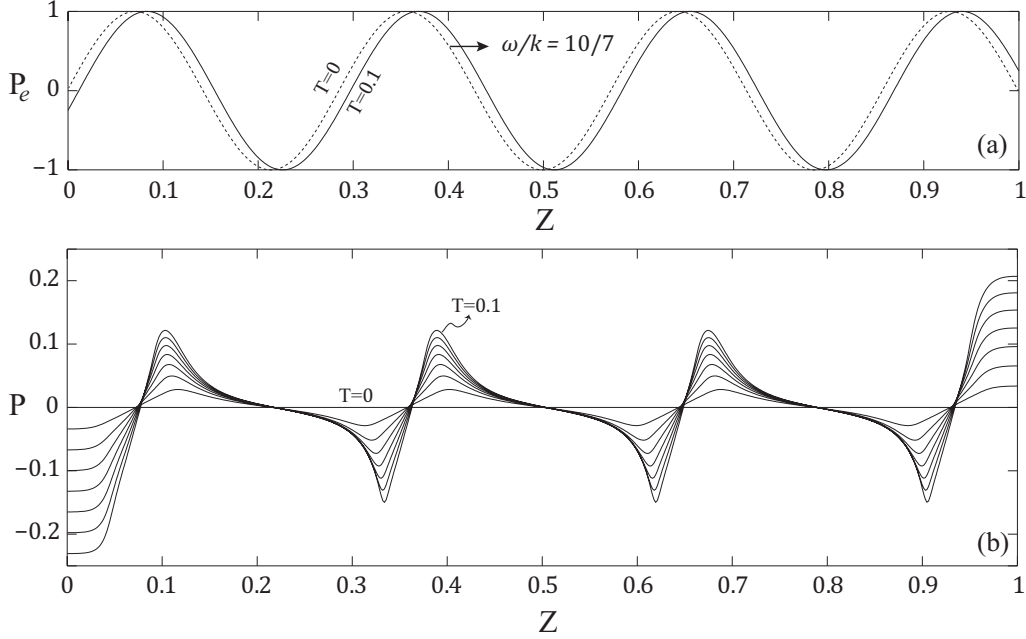


Figure 6: Initial transient phase dipole structure formation in response to an external moving pressure wave. Tube closed at both ends: $\partial P(0, T)/\partial Z = \partial P(1, T)/\partial Z = 0$. Part (a): External pressure $P_e = a \sin(kZ - \omega T)$, $a = 1$, $k = 7\pi$, $\omega = 10\pi$, $0 \leq T \leq 0.1$. Part (b): Fluid pressure in $\Delta T = 0.014$ increments between $0 \leq T \leq 0.1$.

and a no flux condition at the right boundary,

$$P(Z, 0) = 0, \quad \frac{\partial P(1, T)}{\partial Z} = 0. \quad (7.3)$$

Under the above conditions a sequence of symmetric ZKB profiles will propagate through the interface. Assuming sufficiently small λ_h , their compact support is maintained under transport, that is, each pulse is independent and generally does not interact with neighboring pulses. The rate of diffusion of the profiles decays strongly beneath a certain amplitude (determined by (3.36)) and is significantly slower than the rate of their transport, that is, they maintain their form as they are transported. Using this approach, isolated fluid segments can be generated arbitrarily and transported along the interface independent of the pressure gradient and having limited or negligible communication with each other. In particular, the boundary sequence (7.2) can be modulated to form a moving wave signal, as illustrated in Fig. 7 via numerical solution of (7.1)-(7.3). A pre-wetting layer of $\lambda_h = 0.15$ was used with a constant centre-body motion of $U_0 = 2$. Fig. 7(b) shows 3 progressive snapshots of the resulting radial deformation wave at times $T = 0.9, 0.92, 0.94$, as it propagates the interface. The corresponding fluid pressure contour is plotted in Fig. 7(a) and shows the uniformity of the sequence beyond an early generation time, $T > 0.35$. The obtained solution closely approximates the waveform,

$$D_r(Z, T) \approx \frac{A}{2} [1 + \sin(KZ - \Omega T)], \quad \frac{\Omega}{K} = \frac{U_0}{2}, \quad (7.4)$$

where $A = 0.1$ and $K = \Omega = 10\pi$.

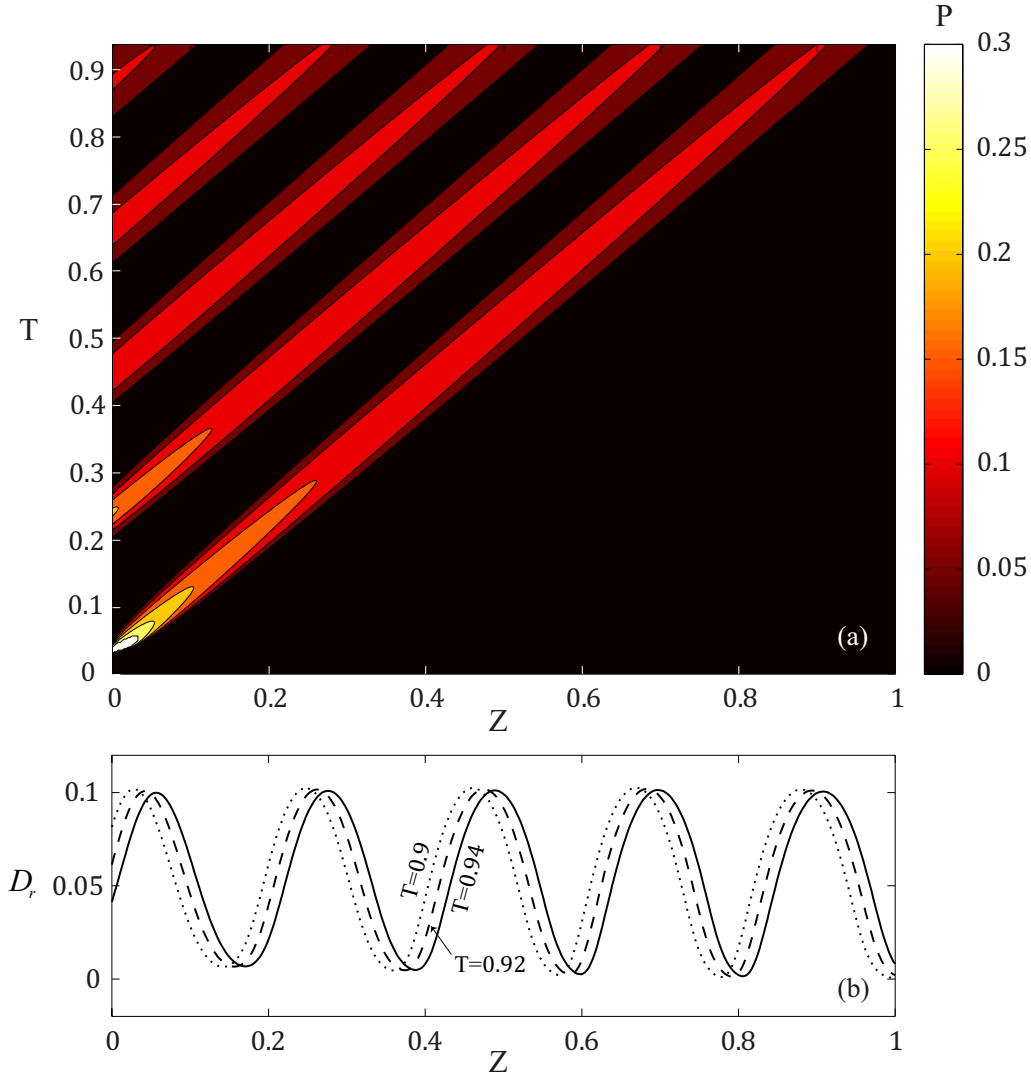


Figure 7: Moving wave deformation pattern generated via a modulated impulse sequence (7.2). A pre-wetting layer of $\lambda_h = 0.15$ is used upon constant centre-body motion of $U_0 = 2$. Modulation laws in the interval $0 \leq T \leq 1$: $A_n = [0.37, 0.54, 0.54, 0.54, 0.54]$, $\tau_n = [0.003, 0.02, 0.0373, 0.055, 0.0732]$, $\Delta T_n = [0.0005, 0.0026, 0.0036, 0.0044, 0.005]$, $n = 1..5$. Part (a): fluid pressure contour in space and time. Part (b): 3 progressive snapshots of the radial deformation wave at times $T = 0.9, 0.92, 0.94$, as it propagates the interface.

8. Concluding remarks

The analysis presented here assumes several small parameters, including geometric requirements such as $\varepsilon_2 = (r_o - r_i)/r_i \ll 1$ and dynamic physical requirements such as small deformations $\varepsilon_3 = d_r^*/r_{b0} \ll 1$ and negligible inertia $Re_r = \rho \varepsilon^2 r_{b0}^2 p^{*5} / \mu^2 (E \varepsilon_2)^4 \ll 1$. While the geometric requirements are given and constant for a specific configuration, the physical requirements depend on, and limit the magnitude of, the characteristic driving

pressure. To illustrate the maximal allowable pressures and characteristic time-scales we examine several configurations with constant geometric ratios $\epsilon = \epsilon_2 = 0.1$. For water ($\mu = 10^{-3}[Pa \cdot s]$, $\rho = 10^3[Kg/m^3]$) as the liquid and rubber ($E = 10^9[Pa]$) as the tube, we obtain $p^* = 10^4[Pa]$, $t^* = 10^4[s]$ in the case of $r_{b0} = 1[m]$ and $p^* = 6.3 \cdot 10^4[Pa]$, $t^* = 4[s]$ in the case of $r_{b0} = 10^{-2}[m]$. For silicon oil ($\mu = 10[Pa \cdot s]$, $\rho = 7.5 \cdot 10^2[Kg/m^3]$) and rubber ($E = 10^9[Pa]$), we obtain $p^* = 4.2 \cdot 10^5[Pa]$, $t^* = 10^2[s]$ in the case of $r_{b0} = 1[m]$ and $p^* = 2.6 \cdot 10^6[Pa]$, $t^* = 0.5[s]$ in the case of $r_{b0} = 10^{-2}[m]$. Hence, a wide range of characteristic driving pressures and time scales can be achieved by varying the properties of the configuration. Unlike linear viscous-elastic dynamics (Elbaz & Gat 2014), the assumption of creeping flow in the current nonlinear problem can be achieved for any configuration, as long as p^* and λ_h are sufficiently small.

Future research may focus on pressure and deformation propagation in cases with varying pre-wetting layer thickness $H_0(Z)$ and centre-body contour $S_b(Z)$. While the governing equation for such configurations is presented in this work (3.34), the current study did not examine solutions for varying $S_b(Z)$ and $H_0(Z)$, these functions may allow for more elaborate control of the deformation field of the external shell. In addition, future research may include the effect of varying external shell thickness, which is similar to spatially varying surface tension, and may allow for transport of isolated deformations without external mechanisms such as presented in §7.

Appendix A. Summary of results in dimensional form

Nonlinear viscous elastic interaction - governing equation in fluid pressure corresponding to (3.34).

$$\begin{aligned} \frac{\partial(p - p_e)}{\partial t} - \frac{r_{b0}^2}{12\mu(E\epsilon_2)^2} \frac{\partial}{\partial z} \left\{ \frac{\partial p}{\partial z} \left(\frac{E\epsilon_2 h_0}{r_{b0}} + p - p_e \right)^3 \right\} \\ + u_0 \left[\frac{1}{2} \frac{\partial}{\partial z} \left(\frac{E\epsilon_2 h_0}{r_{b0}} + p - p_e \right) + \frac{E\epsilon_2}{\epsilon} \frac{ds_b}{dz} \right] \sim 0. \end{aligned} \quad (A 1)$$

Closed-form solution of impulse driven viscous peeling according to self-similarity, corresponding to (4.9).

$$p(z, t) = p^{*\frac{2}{5}} \left(\frac{\kappa\mu(E\epsilon_2)^2}{\epsilon^2} \right)^{\frac{1}{5}} t^{-\frac{1}{5}} \left[1 - \frac{3p^{*\frac{6}{5}}}{40l^2} \left(\frac{\kappa\mu(E\epsilon_2)^2}{\epsilon^2} \right)^{\frac{2}{5}} z^2 t^{-\frac{2}{5}} \right]^{\frac{1}{3}}_+. \quad (A 2)$$

Inlet pressure driven viscous peeling - self-similar propagation laws corresponding to (4.10).

$$z_F(t, \alpha) = l \left(\frac{p^{*3}\epsilon^2 t}{\kappa\mu(E\epsilon_2)^2} \right)^{\frac{1-3\alpha}{2}} \eta_F(\alpha), \quad (A 3a)$$

$$v(t, \alpha) = \frac{2\pi r_{b0}^3}{\epsilon} \kappa^{\frac{5\alpha-1}{2}} (E\epsilon_2)^{5\alpha-2} p^{*\frac{5-15\alpha}{2}} \left(\frac{t}{\mu} \right)^{\frac{1-5\alpha}{2}} Q(\alpha), \quad (A 3b)$$

$$t_b(\alpha) = \frac{\kappa\mu(E\epsilon_2)^2}{p^{*3}\epsilon^2} \eta_F(\alpha)^{-\frac{2}{1-3\alpha}}. \quad (A 3c)$$

v is the interface volume.

This research was supported by the ISRAEL SCIENCE FOUNDATION (Grant No. 818/13).

REFERENCES

- AL-HOUSSEINY, T.T., CHRISTOV, I.C. & STONE, H.A. 2013 Two-phase fluid displacement and interfacial instabilities under elastic membranes. *Physical review letters* **111** (3), 034502.
- BALMFORTH, N.J., CRASTER, R.V. & HEWITT, I.J. 2015 The speed of an inclined ruck. In *Proceedings of the Royal Society of London A: Mathematical, Physical and Engineering Sciences*, , vol. 471, p. 20140740. The Royal Society.
- BARENBLATT, G. I. 1952 On some unsteady fluid and gas motions in a porous medium. *Prikl. Mat. Mekh.* **16**(1), 67–78 (in Russian).
- BUCKMASTER, J 1977 Viscous sheets advancing over dry beds. *J. Fluid Mech.* **81** (04), 735–756.
- CARLSON, A., MANDRE, S. & MAHADEVAN, L 2015 Elastohydrodynamics of contact in adherent sheets. *arXiv preprint arXiv:1508.06234* .
- CHAUHAN, A. & RADKE, C.J. 2002 Settling and deformation of a thin elastic shell on a thin fluid layer lying on a solid surface. *Journal of colloid and interface science* **245** (1), 187–197.
- DUGDALE, D. S. & RUIZ, C. 1971 *Elasticity for engineers*. McGraw-Hill.
- ELBAZ, SB & GAT, AD 2014 Dynamics of viscous liquid within a closed elastic cylinder subject to external forces with application to soft robotics. *J. Fluid Mech.* **758**, 221–237.
- GAD-EL HAK, M. 2002 Compliant coatings for drag reduction. *Progress in Aerospace Sciences* **38** (1), 77–99.
- HALPERN, D & GROTERBERG, JB 1992 Fluid-elastic instabilities of liquid-lined flexible tubes. *J. Fluid Mech.* **244**, 615–615.
- HEWITT, I.J., BALMFORTH, N.J. & DE BRUYN, J.R. 2015 Elastic-plated gravity currents. *European Journal of Applied Mathematics* **26** (01), 1–31.
- HOSOI, A.E. & MAHADEVAN, L. 2004 Peeling, healing, and bursting in a lubricated elastic sheet. *Physical review letters* **93** (13), 137802.
- HOWELL, P.D., ROBINSON, J. & STONE, H.A. 2013 Gravity-driven thin-film flow on a flexible substrate. *J. Fluid Mech.* **732**, 190–213.
- HUPPERT, HERBERT E 1982 The propagation of two-dimensional and axisymmetric viscous gravity currents over a rigid horizontal surface. *J. Fluid Mech.* **121**, 43–58.
- KING, S.E. & WOODS, A. W. 2003 Dipole solutions for viscous gravity currents: theory and experiments. *J. Fluid Mech.* **483**, 91–109.
- LISTER, JOHN R, PENG, GUNNAR G & NEUFELD, JEROME A 2013 Viscous control of peeling an elastic sheet by bending and pulling. *Physical review letters* **111** (15), 154501.
- LOVE, A. E. H. 1888 The small free vibrations and deformations of a thin elastic shell. *Phil. trans. Royal Society A* (179), 491–546.
- MC EWAN, A.D. & TAYLOR, G.I. 1966 The peeling of a flexible strip attached by a viscous adhesive. *J. Fluid Mech.* **26** (01), 1–15.
- MOLLMANN, H. 1981 *Introduction to the theory of thin shells*. John Wiley and Sons.
- MOMONIAT, E. 2006 Axisymmetric spreading of a thin drop under gravity and time-dependent non-uniform surface tension. *Journal of mathematical analysis and applications* **322** (1), 41–50.
- PAIDOUSSIS, M.P. 1998 *Fluid-structure interactions: slender structures and axial flow*, , vol. 1. Academic press.
- PIHLER-PUZOVIĆ, D., ILLIEN, P., HEIL, M. & JUEL, A. 2012 Suppression of complex fingerlike patterns at the interface between air and a viscous fluid by elastic membranes. *Physical review letters* **108** (7), 074502.
- PIHLER-PUZOVIĆ, D., JUEL, A. & HEIL, M. 2014 The interaction between viscous fingering and wrinkling in elastic-walled hele-shaw cells. *Physics of Fluids (1994-present)* **26** (2), 022102.
- TRINH, P.H., WILSON, S.K. & STONE, H.A. 2014a A pinned or free-floating rigid plate on a thin viscous film. *J. Fluid Mech.* **760**, 407–430.
- TRINH, PHILIPPE H, WILSON, STEPHEN K & STONE, HOWARD A 2014b An elastic plate on a thin viscous film. *arXiv preprint arXiv:1410.8558* .

- WHITE, J.P. & HEIL, M. 2005 Three-dimensional instabilities of liquid-lined elastic tubes: A thin-film fluid-structure interaction model. *Physics of Fluids (1994-present)* **17** (3), 031506.
- ZELDOVICH, YA.B. & BARENBLATT, G. I. 1957 On the dipole-type solution in the problems of a polytropic gas flow in porous medium. *Prikl. Mat. Mekh.* **21**, 718–720 (in Russian).
- ZELDOVICH, Y.B. & KOMPANEETS, A.S. 1950 Towards a theory of heat conduction with thermal conductivity depending on the temperature. In *Collection of Papers Dedicated to 70th Anniversary of A. F. Ioffe*. **1**, 61–72.